EMI Generated EOS in a Wire-bonder

Icko Eric Timothy Iben (1), Vladimir Kraz (2), Michelle Lam (3), Daniel P. Brown (3)

(1) IBM Co, Tape Head Development , 650 Harry Rd., Almaden Research Center, Bldg 80, D2-244, San Jose, CA 95120-6099, USA. tel.: 408-927-1386, e-mail: iben@us.ibm.com

(2) OnFILTER, Inc., 730 Mission St., Santa Cruz, CA 95060 USA
tel.: 831-824-4052, fax: 206-350-7458, e-mail: vkraz@onfilter.com

(3) IBM Co, Tape Head Characterization, 855 Embedded Way., Bldg 52, 1A068, San Jose, CA 95138-1030, USA.
tel.: 408-705-9599, e-mail: lammi@us.ibm.com and dpbrown@us.ibm.com

Abstract–Wire-bonding equipment is essential to modern electronics manufacturing lines. Equipment, such as motors, either from components within or external to the wire-bonder can generate EMI. This is a study of EMI on a wire-bonder, determining the EOS levels, the potential for damage to sensitive electronics devices and means of eliminating the unwanted EMI.

I. Introduction

Automated wire-bonding equipment is essential to modern electronics manufacturing lines. The lifeblood of the electronics industry is continual increasing of the number of elements per wafer, which in turn requires the shrinking of the device size. The smaller the device, the more sensitive to EOS damage. For example, TMR sensors used in the storage industry are sensitive to dielectric breakdown. Damage from voltages as low as 600 mV for a 10 ns window have been reported on TMRs used in the hard disk drive (HDD) industry as read elements [1]. In the study by Chen et al, the TMR devices had a tunnel barrier thickness of 6 Angstroms and an average resistance measured at low currents of 400 Ω. At elevated bias voltages in ESD/EOS events, the TMR resistance decreases to about 50% the cold resistance, [2], so the damage currents were of the order of 3 mA. Current pulses with a width of 3 ns and a level of 3 mA have been recorded in a wire-bonding tool [3]. Thus, it is essential to find the sources of the current pulses and to eliminate or diminish them for use with such sensitive devices. Since the read elements are wire-bonded to a cable to enable use in a read-write drive, it is essential that the wire bonder is made safe for such sensitive devices. In this study, we will evaluate the potential for EMI as the source of the pulses and offer a solution to eliminating EMI as a source of EOS damage in a wire-bonding tool.

While this paper focuses on EMI-caused EOS in magnetic recording, it is also applicable to any semiconductor device in wire bonding process.

II. EOS Pulses in a Wire-Bonder Tool

Figure 1a shows a picture of a wire-bonder tool. The setup shows the wire-bonding finger touching the pads of a printed circuit board, PCB. Resistors were wired to the pads of the PCB and a CT1 Current probe (Tektronix, 25 kHz to 1 GHz) was inserted in the circuit to measure current pulses during wire-bonding. Figure 1b shows the circuit for measuring the current pulses. In a previous study [3], a total of 65 touches were analyzed for registering pulses. The trigger threshold was set at 1 mA, and in 15 out of the 65 touches (23%), currents >1 mA were recorded. The average current level measured was 2.4 mA with a standard deviation of 0.6 mA and a maximum of 3.7 mA. Assuming a Gaussian distribution, the 3-sigma current level is 4.2 mA. Thus, 1 out of every 4000 touches will be of the level of 4.2 mA. A major unknown is the source of the current pulses.

III. EMI Pulses in a Wire-Bonder Tool

Figure 2 is a photograph of the wire bond station and experimental setup used to measure EMI on the wire-bonder finger. A Hantek DS01200 portable oscilloscope and a Tektronix CT1 current probe were used to capture current pulses. The oscilloscope had a 200 MHz band width, sample rate of 500MS/sec. The CT1operates between 25 kHz to 1 GHz and has a 5 mV/mA output. The wires connected the ground plate

and the finger of the wire-bonder tool together using a special test fixture that allowed current measurements with and without an EMI suppression filter.

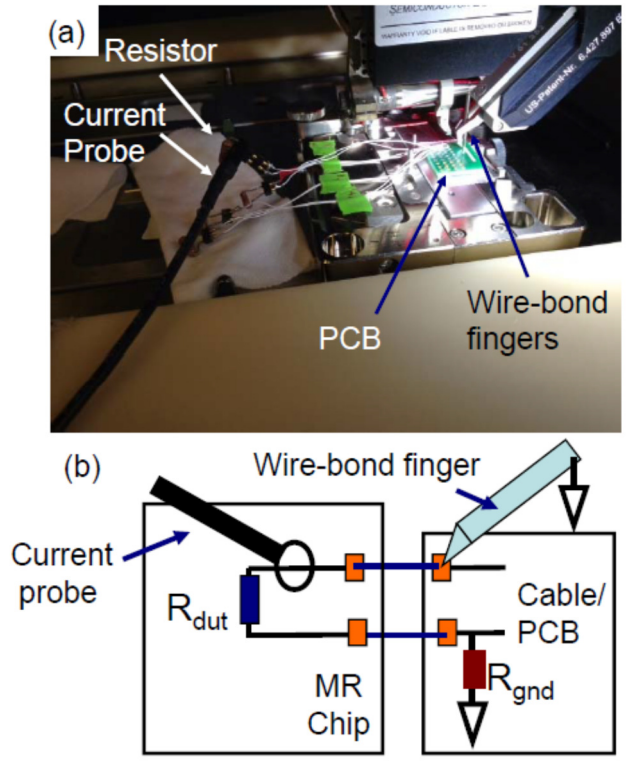

Figure 1. (a) Photograph of wire bond station and experimental setup used to measure spurious pulse occurring during wire bonding (b) Circuit for measuring current pulses.

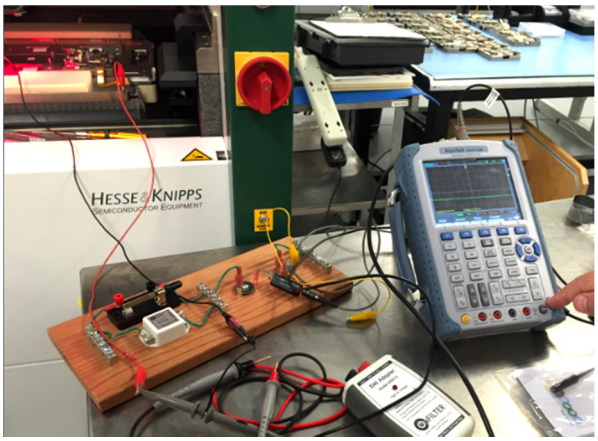

Figure 2. Photograph of wire bond station and experimental setup used to measure EMI on the wire-bonder finger.

Figure 3 shows an equivalent circuit of the measurement setup. A source of EMI (voltage source) has an output impedance, Z_{out} and is connected in series with the test leads and a wire going through current probe. Filter is bypasses by a switch to measure filter's effectiveness. All impedance components are shown regardless of their significance in this case as in other circumstances their values may be different.

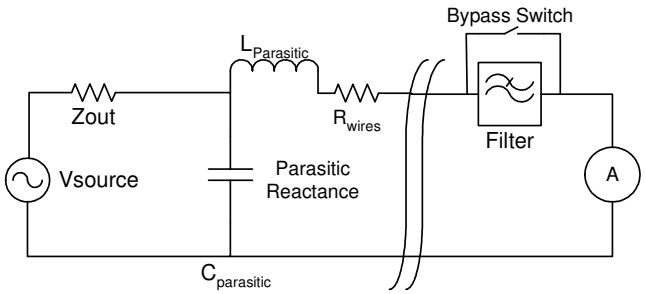

Figure 3. Equivalent circuit of the current measurement.

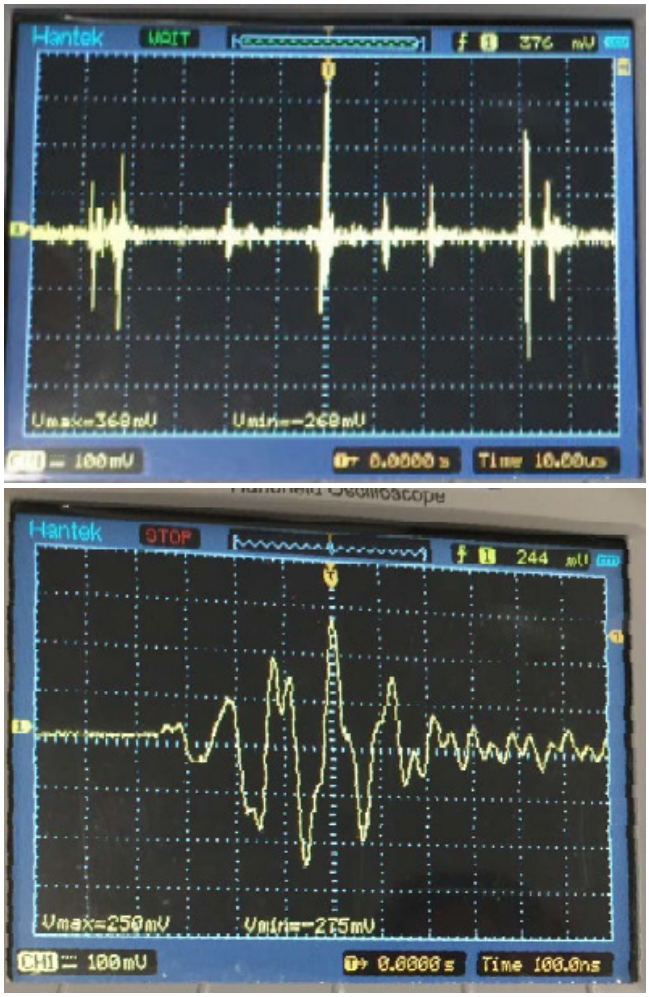

Figure 4. Photograph the recorded voltages between the ground plate and the finger of the wire-bonder tool (direct connect). (a) 10 µs/div (b) 100 ns/div. Both were 1 V /div.

Figure 4a shows recorded EMI voltage for a direct wire connection between the wedge and ground at 10 µs/division and 100 mV/division. Voltage bursts were observed at between 10 to 20 µs intervals with peak currents of 10s of mA (CT1 is 0.2 A/V). Figure 4b focuses in on the individual voltage pulses, using 100 ns/division. The bursts had ringing/oscillations with a period of ~120 ns (8.3 MHz). The full width at half maximum, FWHM, of the oscillations was about 20 ns. It is expected that oscillations are likely to be a

contribution of parasitic reactance of the test leads and impedance mismatch at high frequencies.

Transients on ground are caused by sharp edges of pulses - usually, drive pulses of servo motors or switching pulses of SMPS (switched mode power supply). Sharp edges of these pulses cause corresponding spikes on power lines and ground via capacitive coupling, leakage currents, or other means, where they pollute equipment ground with electrical noise. Servo motors, and their cousins, variable frequency motors (VFD), typically use pulse repetition rate of 6 to 25kHz while switched SMPS operate from 20kHz and up, mostly up to 200kHz. Keeping in mind that the transients may manifest themselves on both rise and fall times of the originating pulses, there is an overlap in repetition rate between servo motors and SMPS. In our case the pulse repetition rate is 45 kHz (Figure 4a) which may fall either in the domain of SMPS or of servo motor drive signal due to doubling pulse repetition rate on the rise and fall. More work will be done on diagnostics of the origins of the strongest pulses found on ground of the bonder.

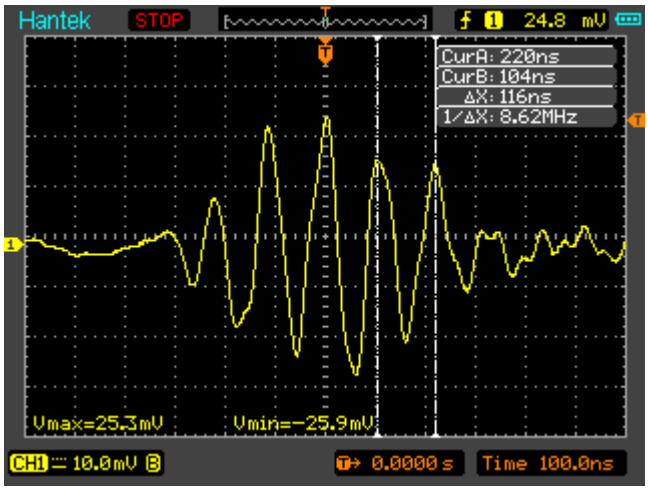

Figure 6. Current (a) measured and (simulated) with R_{dut} of 0.1 Ω and C1 of 118 pF labeled F01, F02 and F08 in Table 1.

In order to understand the currents measured, the currents were measured using different load impedances. The loads consisted of a resistor (R_{dut}) and capacitor (C1) connected in series between the wedge and the system ground. Figures 6 and 7 plot the current measured with R_{dut} of 0.1 Ω (short) and C1 of 24 pF and 118 pF and are respectively labeled F07 and F08 in Table 1, which summarizes the oscillation frequency, f, and the peak currents for the various circuits studied. Note that the exact shape and the amplitudes vary, though the oscillation frequencies are generally repeatable.

Table 1. Summary of peak-to-peak currents, I_{peak}, and oscillation frequency, f, for different values of R_{dut} and C1. For the simulations (Sim), V1 of 2 V is used

				frequency		Peak Current	
	C1	R_{dut}	Filter	Data	Sim	Data	Sim
Case	pF	Ω	Yes/ No	MHz	MHz	mA	mA
F01	118	0.1	No	9.3	11.1	12.3	17.4
F02	118	0.1	No	9.3	11.1	13.1	17.4
F03	118	0.1	Yes	x	x	0	0
F04	-	0.1	No	7.6	6.9	31.8	41.4
F05	-	0.1	Yes	x	x	0	0
F06	24	0.1	No	21.7	20.5	9.5	7.4
F07	24	0.1	No	21.7	20.5	9.4	7.4
F08	118	0.1	No	8.6	11.1	10.3	17.4
F09	-	499	No	9.4	*	3.8	6.2
F10	-	50	No	9.6	11.7	16.0	23.6
F11	24	50	No	25	20.5	5.3	6.1

x No signal, so no observed oscillations, an no simulation performed

* Over-damped, so no oscillations observed in simulations

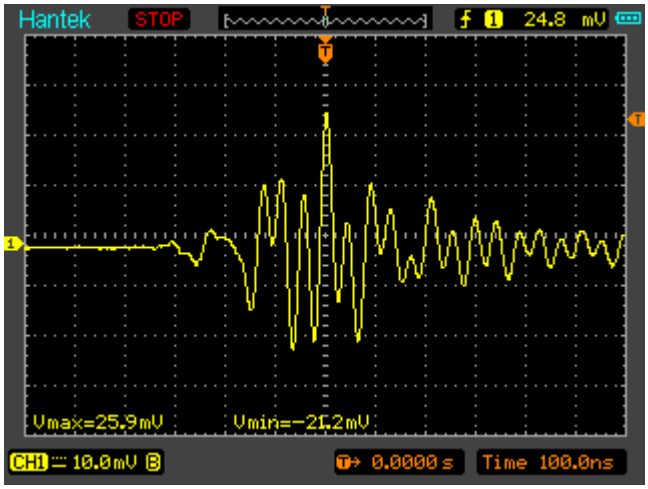

Figure 7. Current measured with R_{dut} of 0.1 Ω and C1 of 24 pF labeled F06 and F07 in Table 1.

Figure 8 (F10) shows the effect of a higher value for R_{dut} of 50 Ω without a series capacitor. With the added purely resistive load, the oscillations are primarily a single frequency of about 9.6 MHz and a peak-to-peak current of about 16 mA.

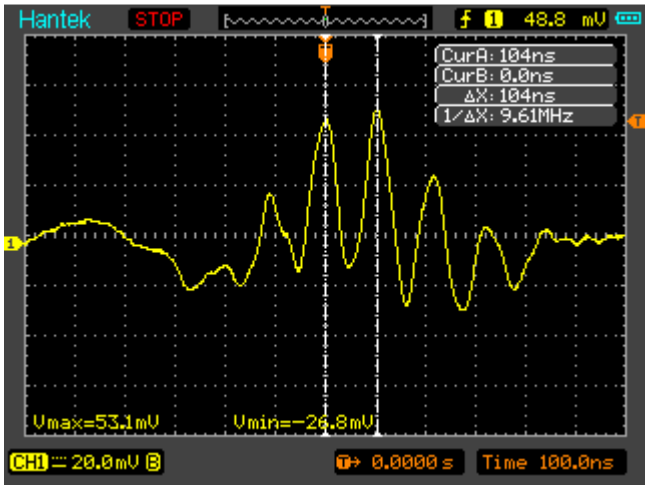

Figure 8. Current measured with R_{dut} of 50 Ω , without a series capacitance labeled F10 in Table 1.

Figure 9 (F11) shows the addition of a series capacitance, C1, of 24 pF. The oscillations are more complex, but contain a frequency of about 21 MHz, and a reduced peak-to-peak current of about 5.3 mA.

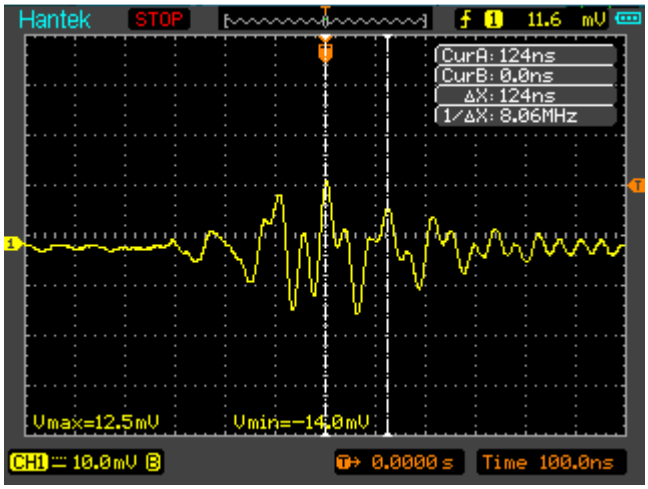

Figure 9. Current measured with R_{dut} of 50 Ω and C1 of 24 pF labeled F11 in Table 1.

IV. EMI Circuit Model

In this section, we will propose a circuit model and collect data to determine the parameters. Figure 10 is the model proposed. V1 is the source or the voltages, presumably originating from the stepper motor driver. The pulse will be taken as a voltage step with a rise, fall and duration. The values chosen for the simulations were 20 ns rise and fall times and a duration of 180 ns. The capacitor C2 represents the coupling between the stepper motor and the wire-bonder wedge. R_{wire} is the high frequency resistive component of the circuit, which is several ohms and L2 is the inductance of the system, which as will be shown later is on the order of µHs. R_{dut} and C2 are the values of resistance and capacitance introduced into the circuit in an attempt to better understand the circuit. For a short, R_{dut} is taken as 0.1 ohms, as R_{wire} takes into account the system resistance. For a short, C2 is taken to be 1 µF, which is a short for pulses in the 10 MHz range.

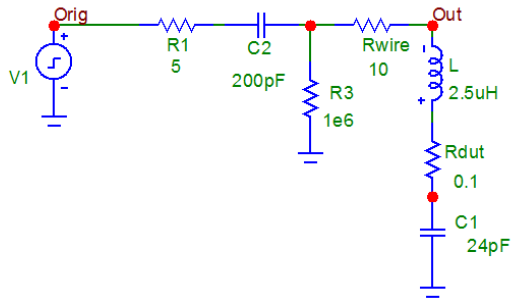

Figure 10. Equivalent circuit for simulating EMI for Fig 4b.

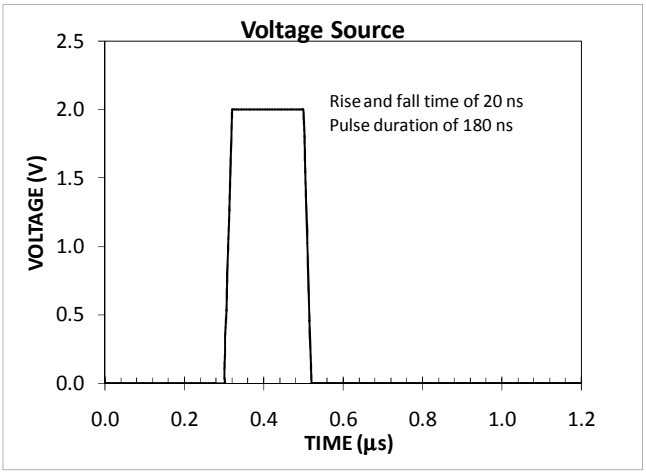

Figure 11. Voltage source, V1, used for the simulations.

Figure 11 is a plot of the voltage source, V1, in Figure 10. A 20 ns rise and fall time and a 180 ns duration are used. The magnitude of the voltage source, V_{so}, is taken as 2 V. In reality, the rise time may be of the order of 20 ns. The actual pulse shape, though, is more likely a decaying pulse from an LRC coupling. Also, due to the capacitive coupling (C2), the rise and fall times affect the peak-to-peak current, with the current peak increasing the shorter the rise time. The rise and fall time and the pulse duration were chosen to most closely approximate the measured pulse shapes and magnitudes.

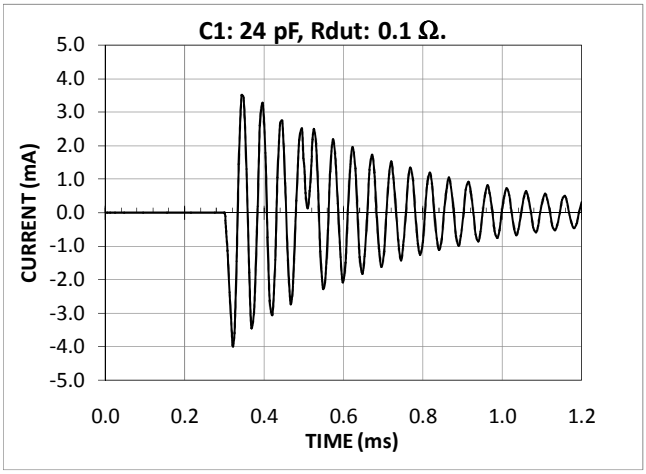

Figure 12. Simulation results: current through R_{dut} of 0.1 Ω and C1 of 24 pF labeled F06 and F07 in Table 1.

Figure 12 is the results of the simulation using the circuit in Figure 10 with the voltage source in Figure 11 for an R_{dut} of 0.1 Ω and C1 of 24 pF, and the results are given in Table 1 for F06 and F07. The simulation frequency of 20.5 MHz is close to the measured value of 21.7 MHz, and the peak-to-peak current of 7.4 mA is 21% lower than the measured value, which is within the experimental reproducibility.

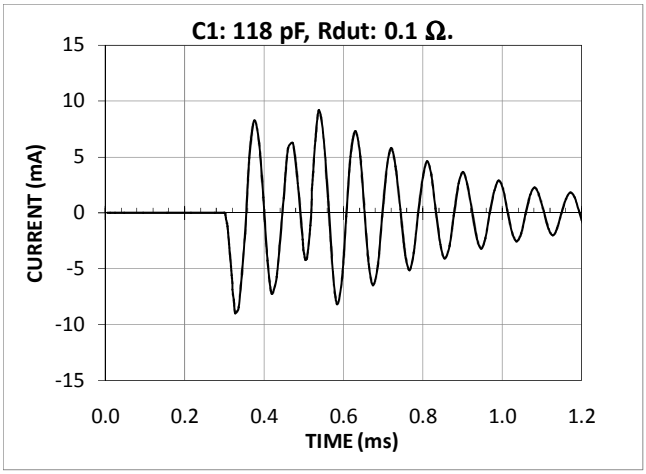

Figure 13. Simulation results: current through R_{dut} of 0.1 Ω and C1 of 118 pF labeled F01, F02 and F08 in Table 1.

Figure 13 is the results of the simulation for an R_{dut} of 0.1 Ω and C1 of 118 pF, and the results are given in Table 1 for F01, F02 and F08. The simulation frequency of 11.1 MHz is close to the measured value of 9.0 ± 0.4 MHz, and the peak-to-peak current is 46% higher, which is within the experimental reproducibility. The standard deviation and range of the peak-to-peak currents of the data recorded were 12% and 24% respectively. Actual data variations were noted to be as large as +100% and -50%, but given the limited time allowed on the production tool, we were unable to get sufficient measurements for accurate statistics.

Figure 14 is the results of the simulation for an R_{dut} of 50 Ω and C1 of 24 pF, and the results are given in Table 1 for F11. The simulation frequency of 20.5 MHz is close to the measured value of 25 MHz. Note that the actual oscillations shown in Figure 9 are clearly not a single frequency, and indicate a more complex circuit. The peak-to-peak current of 6.1 mA is only 15% higher than the reported 5.3 mA.

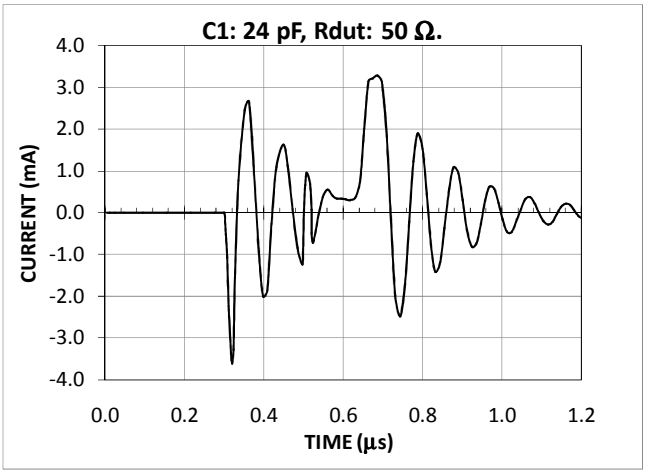

Figure 14. Simulation results: current through R_{dut} of 50 Ω and C1 of 24 pF labeled F11 in Table 1.

V. Analysis of the LRC Circuit

By modifying the values of R_{dut} and C1, one can gain a better insight into the circuit model. Table 1 gives a summary of important parameters for different values of R_{dut} and C1. Changes in R_{dut} and C1 result in changes of both the current magnitude and the frequency of the response. The essence of the changes can be understood from a simple LRC model in response to an impulse voltage source. Equation 1 gives Ohm's law:

$$\frac{Q}{C} + R\dot{Q} + L\ddot{Q}=0 \quad (1a)$$

$$I(t) = \dot{Q} = w_r C V_{so}\left[1 + \frac{1}{(w_r\tau)^2}\right]\sin(w_r t)e^{-t/\tau} \quad (1b)$$

$$w_r = 2\pi f = \sqrt{\frac{1}{LC} - \left(\frac{1}{\tau}\right)^2} \quad (1c)$$

$$\tau = \frac{2L}{R} \quad (1d)$$

R is simply the series of R1, R_{wire} and R_{dut}:

$$R = R_1 + R_{wire} + R_{dut} \quad (1e)$$

C is the series connection of C1 (dut-to-fixture capacitance) and the capacitance C2 connecting the source voltage to the wedge:

$$\frac{1}{C} = \frac{1}{C1} + \frac{1}{C2} \quad (1f)$$

The choice of parameters is dictated by the oscillation frequency, f, and the damping coefficient, τ.

The current magnitude, then can be varied by the value of V_{so}.

An estimate of the inductance, L, can be made assuming the wires shown in Figure 2 form a rectangle with a length l_w of 0.6 m and a separation, s_w, of 7 cm, and the wires have a radius, r_w, of 0.25 mm:

$$L = \left[\frac{2\mu_o}{2\pi}\right]\left[l_w ln\left(\frac{s_w}{r_w}\right) + s_w ln\left(\frac{l_w}{r_w}\right)\right] \qquad (2)$$

μ_o (=4πx10^{-7} H/m) is the permeability of air. Using the approximate values given above yield an L of 1.6 μH, which is close to the value of 2.5 μH used to fit the data.

A note of capacitance values for C1 in the wire-bonding of actual parts. For an example, take the wire-bonding of a wafer level semiconductor or magnetic read/write element to a flexible cable. For a cable having a lead with of W_L and a thickness of d such that the cable is mounted on a grounded fixture, then for a lead length, L, the capacitance between the lead and ground, C_L, is:

$$C_L = {\varepsilon_k \varepsilon_o W L}/{d}. \qquad (3)$$

ε_o is the permittivity in a vacuum (8.95 pF/m) and ε_k is the relative permittivity of the cable substrate. A representative lead width is 100 μm. The leads are encased in Kapton or other plastic material, with thicknesses on the order of 10 μm. Kapton has a permeability, ε_k, of the 3.5 [4]. A typical Kapton thickness is about 12 μm. Using the cable values given above, a representative C_L is 2.6 pF/cm. For a 5 and 10 cm long lead, C_L is 13 and 26 pF respectively.

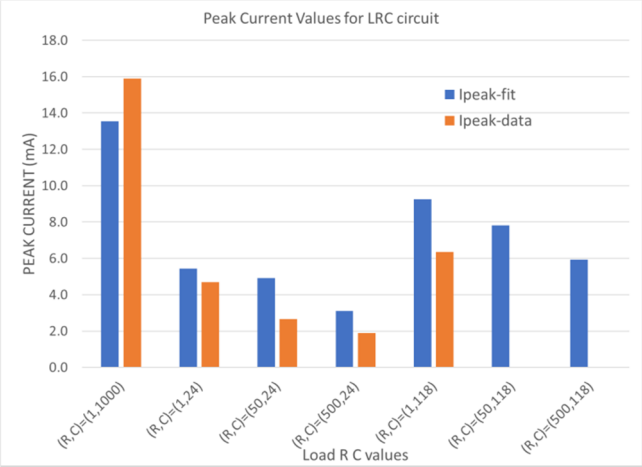

Figure 15. Bar chart of the measured and fit current through R_{dut} for various values or R_{dut} and C1.

Figure 15 is a bar plot of the measured current through R_{dut} versus different values for C1 and R_{dut}. Also, In the fits, V_{so}=2 V, $C_{fixture}$ is taken as 5 pF, R_{wire} is 10 Ω, L 2.5 nH and C2 is 200 pF.

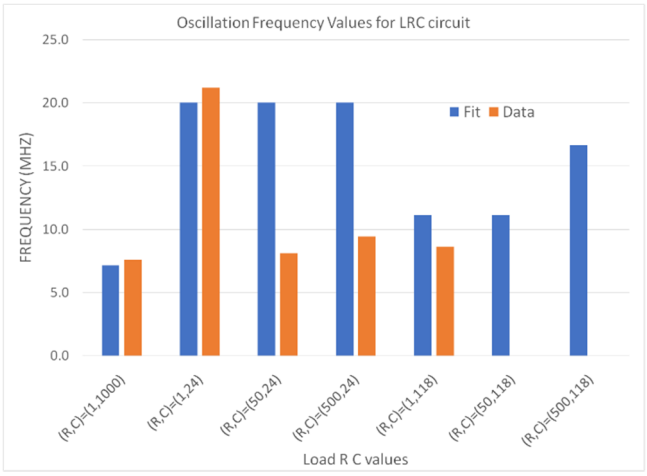

Figure 16. Bar chart of the measured and fit oscillation frequency for various values of R_{dut} and C1.

VI. Elimination of the EMI Using an EMI Filter

The high-frequency (EMI) currents may be sufficiently blocked using a high frequency filter [5] Figure 4 shows the setup used to test the currents with and without an EMI filter. In Figure 2, the switch is connected, bypassing the EMI filter. The bypass switch of Figure 2 is now open, so the current passes through the EMI filter. For these experiments, ground line EMI filter GLE04-01 from OnFILTER [6] was used. Within the noise of the system, no noticeable current or artifacts were observed. Figure 17 shows the resulting current when a direct short connected the wedge to ground (F01) or a 118 pF capacitor was used. Absolutely no currents were observed within the noise of the system, and we were forced to do a manual trigger to collect the data.

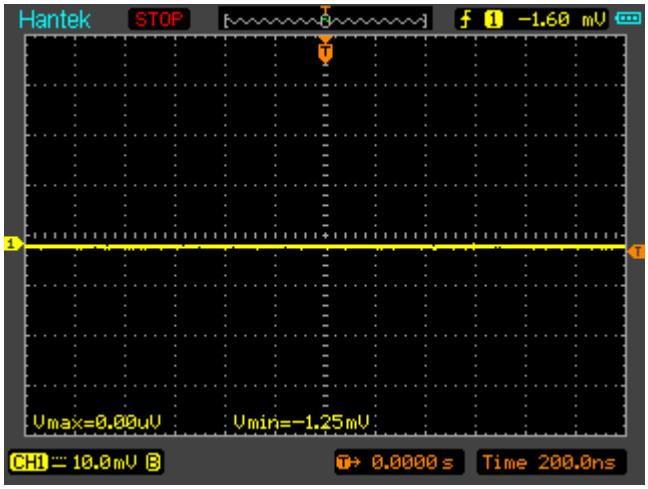

Figure 17. Current with EMI filter. (F03 or F01)

VII. Wire-bonding to an MR head

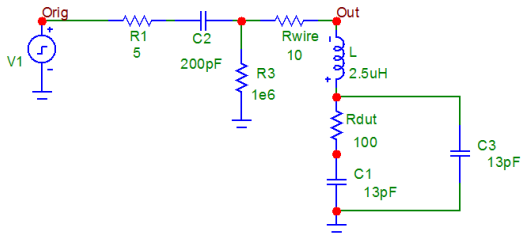

Figure 18. Circuit to for wire-bonding to an MR element.

Figure 18 shows an equivalent circuit to bond to an MR head. The capacitive coupling between the MR head and the ground plane is taken to be 24 pF, and the capacitance is taken to be divided evenly between the two ends of the MR leads, each with the calculated capacitance of 13 pF. The MR element, (R_{dut}) is taken to have a resistance of 100 Ω. For current to pass through R_{dut}, one cable lead must already be bonded to R_{dut}. When the wedge contacts the 2nd lead to to R_{dut}, current can pass through either C3 or R_{dut} and C1. Figure 19 plots the resulting current through R_{wire} and R_{dut}. The simulation shows that half the current passes through C1 and the other half through C3. The oscillation frequency is 20 MHz. The peak positive and negative current values passing through R_{dut} are -2.0 and +1.6 mA respectively, and is half the total current. The explanation for half the current passing through R_{dut} is that the impedance of a 13 pF capacitor at 20 MHz is 612 Ω, which is significantly higher than the value for R_{dut}. Even with an R_{dut} of 500 Ω, the current passing through R_{dut} is close to 50% of the total current, and is calculated to be -1.6 and +1.7 mA.

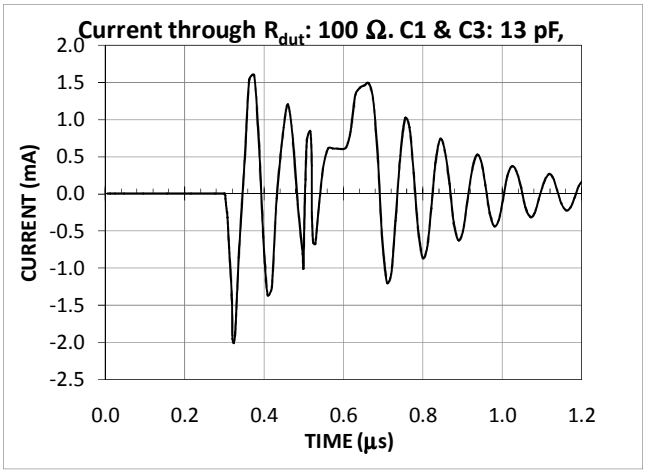

Figure 19. Plot of the current through an R_{dut} of 50 Ω using the circuit and circuit parameters given in Figure 18.

Varying the values of C1 and C3 will change the current, I_{dut}, through R_{dut}. Tables 2a and 2b respectively gives the maximum for I_{dut} versus C1, with C3 equal to C1 for an R_{dut} of 100 Ω and 350 Ω. The voltage across the DUT is also given, as the dielectric breakdown of TMR elements is primarily a voltage driven event. The oscillation frequencies given in Tables 2a and 2b are equivalent to pulses of the order of about 2 to 20 ns. TMR elements used for magnetic recording with a resistance of 100 Ω have tunnel barriers of the order of 13 nm, and breakdown voltages for the 2 to 20 ns range over 1.2 V [2], so damage from the wire-bonder for such parts is not expected. For a TMR with a thickness of 5 nm and a resistance of the order of 350 Ω, the breakdown voltage at 2.3 ns is reported to be 630 mV. Using the linear extrapolation for lifetime of the data published, the breakdown voltage for a 10 ns pulse is extrapolated to be about 270 mV [1]. Using the projections from Table 2b, with capacitive coupling values of C1 and C3 of between 10 to 20 pF, damage can occur to TMR sensors with thicknesses of about 5 nm and resistances of about 350 Ω.

Table 2a. I_{dut} and f versus C1 & C3 using the circuit in Figure 18 with an L of 2.5 µH and R_{dut} of 100 Ω.

C1,C3	pF	1	5	10	20	50
f	MHz	67.6	34.7	22.4	16.8	11.8
1/(8*f)	ns	1.8	3.6	5.6	7.4	10.6
I_{dut}	mA	0.23	0.95	2.2	2.9	4.8
V_{dut}	mV	23	95	220	290	480

Table 2b. I_{dut} and f versus C1 & C3 using the circuit in Figure 18 with an L of 2.5 µH and R_{dut} of 350 Ω.

C1,C3	pF	1	5	10	20	50
f	MHz	68.5	30.9	27.5	17.6	12.9
1/(8*f)	ns	1.8	4.0	4.5	7.1	9.7
I_{dut}	mA	.19	.82	1.5	2.3	3.1
V_{dut}	mV	67	287	525	805	1085

Note that the duty cycle of the bursts is low, with a burst occurring once every 20 µs, and the peak pulses lasting several 10s of ns. This duty cycle must be taken into consideration when determining the probability of a pulse occurring during any wire-bond step. One of the authors mentioned that the time which the finger remains in contact for a wire bond is of the order of 20 to 30 ms, so with a burst every 20 µs, the TMR will be subjected to between 1000 and 1500 pulses, greatly reducing the sensitivity level.

VIII. Discussion

Motors can generate the observed EMI (8 to 20 MHz). We have shown that the EMI pulses can be simulated using a reasonable circuit. We have also

shown that the EMI pulses can be significantly reduced by using an EMI filter. Further work is needed for connecting the observed EMI pulses with the measured pulses during wire-bonding. Further circuit simulations to fit the EMI signals with varying values of L, C1 and R_{wire} will be useful. We also intend to determine whether the pulses observed during wire-bonding are eliminated or reduced using the EMI filter. This question can be addressed by repeating the voltage pulses with and without the filter. While the oscillations measured in the EMI experiments were of significantly different width and duration to the pulses measured in the wire-bonding experiment, this is not unreasonable, since the wires used to measure the EMI added significant induction to the circuit, and the wire-bonding circuit used a large resistor (100 Ω) in series with L. Lowering L will decrease the oscillation period, and adding a large resistor in series with L1 will dampen the oscillations. A direct test would be to add the EMI filter directly into the wire-bonding circuit and to repeat the wire-bonding current pulse measurements. This will involve modifying the wire-bonder, which we did not have time to do for the paper.

IX. Conclusion

In this paper, we have measured EMI in a wire-bonding tool which is similar in nature to direct pulses measured during wire-bonding. Presented signals represent the worst-case EMI current exposure. Overall signal properties measured in the EMI were similar to the EOS pulses measured during wire-bonding. The high-frequency EMI currents can be blocked using a ground line EMI filter.

Acknowledgements

Tim Iben and Michelle Lam want to thank their managers, Gary Decad and Darren Ellenburg for their support of this work.

References

[1] T W Chen, A Wallash, R W Dutton, “Ultra-Fast Transmission Line Pule Testing of Tunneling and Giant Magnetoresistive Recording Heads”, EOS/ESD Symposium., pp 258-261 (2008).

[2] I. E. T.Iben, “Dielectric Breakdown of TMR Sensors and the Role of Joule Heating", 2A.3 (2016).

[3] I. E. T.Iben, P Golcher, M. Lam, M. Mohammadnejad and Bill Paniagua, “Auditing of a Class 0 Facility”, EOS/ESD Symposium, 7B.2 (2013).

[4] DUPONT™ KAPTON ® "Summary of properties", http://www.dupont.com/content/dam/dupont/ products-and-services/membranes-and-films/polyimde-films/documents/DEC-Kapton-summary-of-properties.pdf

[5] Complete Grounding Inside Equipment for Combined ESD and EOS Protection, Application Note, OnFILTER

[6] Ground line EMI filterGLE04-01 from OnFILTER